

Cyclic voltammetry and scanning electrochemical microscopy of ferrocenemethanol at monolayer and bilayer-modified gold electrodes

Céline Cannes^{a,*}, Frédéric Kanoufi^b, Allen J. Bard^a

^a Department of Chemistry and Biochemistry, The University of Texas at Austin, Austin, TX 78712, USA

^b Laboratoire Environnement et Chimie Analytique, UMR 7121, ESPCI, 10 rue Vauquelin, 75231 Paris Cedex 05, France

Received 22 October 2002; received in revised form 11 February 2003; accepted 1 March 2003

Abstract

Ferrocenemethanol was chosen to study quantitatively the kinetics of the heterogeneous electron transfer at mono- and bilayer-modified gold electrodes. The monolayer was prepared by tetradecanethiol adsorption on the gold surface and the bilayer was formed by phospholipid adsorption on the first layer. The apparent electron transfer rate constants at the modified gold electrodes were measured by cyclic voltammetry (Tafel analysis) and from scanning electrochemical microscopy approach curves, as well as by simulations of the cyclic voltammograms. The values obtained by simulation based on a CEC mechanism were close to the values obtained by both other techniques. The results show that the surface coverage was high and depended on the thickness of the layer (0.993 for the monolayer and 0.9998 for the bilayer). The major consequence of this high coverage is a large decrease in the apparent rate constant for ferrocenemethanol oxidation that depended on the thickness of the modifying layer. The results also indicate that ferrocenemethanol could permeate to a small extent into the monolayer. The electron transfer at the bilayer is mainly governed by diffusion of the mediator through pinholes with electron transfer occurring at the free sites on the electrode rather than permeation. © 2003 Elsevier Science B.V. All rights reserved.

Keywords: Monolayer; Bilayer; Gold electrode; Mass transport; Cyclic voltammetry; SECM

1. Introduction

A better understanding of ion and electron transport through membranes is crucial in elucidating the mechanisms involved in many biological systems, e.g. cellular energy production by respiration and photosynthesis or signal transmission in nerve systems. For a quantitative analysis, as these systems are often complex, simpler, better defined and more easily interpretable models are needed. Biomimetic membrane systems include vesicles [1], bilayer lipid membranes [2] and solid-supported lipid layers [3]. The latter can be prepared by Langmuir Blodgett techniques [4], by fusion of vesicles [5], by lipids adsorbed on fresh cut metal surfaces [6], or by self-assembly [7–21]. The easy preparation and the high stability of the bilayer make the self-assembly method very attractive for the preparation of modified surfaces.

Another advantage of this method is that the bilayer is formed on a conductive support that allows surface and electrochemical analysis. When such an immobilized monolayer or bilayer is formed and electrochemical studies of species dissolved in the solution are undertaken, it is necessary to distinguish between alternative modes of electron transfer. These include electron tunneling through the layer, reaction on the conductive substrate at defects in the layer, and permeation of the species into the layer.

Scanning electrochemical microscopy (SECM) is a powerful technique for studies of topography and electrochemical processes in localized spaces. It has already been used in the case of a solid | liquid interface modified by a film [22–25] or by a monolayer [26–28], of a liquid | liquid interface modified by a monolayer [29] or bilayer [30–32] and of an air | water interface modified by a monolayer [33].

Although electrodes modified by a mono- or bilayer have already been analyzed, only few studies led to a quantitative analysis. Therefore, we have used cyclic

* Corresponding author. Université Paris Sud, I.P.N., Gr. De Radiochimie, Orsay Cedex 91406, France.

E-mail address: cannes@ipno.in2p3.fr (C. Cannes).

voltammetry (CV) and SECM to study quantitatively the kinetics of the ferrocenemethanol electron transfer at a gold electrode modified by a layer. The monolayer preparation consists in the tetradecanethiol ($C_{14}SH$) adsorption on the surface. This layer is very stable as it is covalently bound [34,35], and it provides a hydrophobic surface that allows the adsorption of phospholipids (POPC) to form a bilayer. Then, the first layer is constituted of a long alkane chain and the second layer of a long chain containing several functional groups.

2. Experimental

2.1. Chemical reagents

Tetradecanethiol (Lancaster), ferrocenemethanol (Aldrich), sodium ferrocyanide (Aldrich), sodium chloride (EM) and 1-palmitoyl-2-oleoylphosphatidylcholine in chloroform (POPC, Avanti) were commercial grades and were used without further purification. Ethanol was absolute analytical grade. All solutions were prepared with deionized water (Milli-Q, Millipore Corp.).

2.2. Preparation of the mono and bilayer

The monolayer was prepared according to the method described by Forouzan et al. [26]. The gold disk electrode was a gold wire ($S = 0.038 \text{ cm}^2$) inserted in Teflon. This disk electrode was first polished carefully with 0.3 and 0.05 μm alumina, and sonicated in water for 15 min and then in ethanol for 2 or 3 min. After cleaning the electrode with hot sulfuric acid and rinsing it with water, several scans were made over the range -0.3 – 1.5 V ($\text{Ag} | \text{AgCl}$) in freshly prepared deoxygenated 0.5 M H_2SO_4 . The electrode was rinsed with water, then ethanol, dried in air, and finally immersed in absolute ethanol solution of 5 mM tetradecanethiol overnight. Before electrochemical measurements, the electrode was rinsed with ethanol and dried in a stream of pure nitrogen or argon.

The bilayer was prepared according to the method described by Plant [8]. It consisted in the addition of a vesicle solution (with a final lipid concentration of 0.2 mM) to the cell containing the alkanethiol-coated electrode for 6 h. To prepare the vesicle solution, 160 μl of POPC (10 mg ml^{-1} in chloroform) was dried in a stream of pure nitrogen and then placed in a vacuum desiccator overnight to remove residual chloroform. The lipids were resolubilized in 1 ml of 20 mM tris buffer and 150 mM NaCl, mixed for 5 min with a vortex mixer and sonicated for 40 min. Before measurement, the cell was rinsed several times with water and with the ferrocenemethanol solution to remove excess vesicles. This step had to be carried out carefully, since the bilayer can be

disturbed if the electrode surface comes in contact with air.

2.3. Measurements

Electrochemistry experiments were carried out with a CHI-900 electrochemical workstation (CH Instruments, Austin, TX), employing a three-electrode cell with a gold working electrode, a platinum wire counter electrode and a Ag wire reference electrode ($E_{\text{Ag}} = -0.073 \text{ V}$ vs. $\text{Ag} | \text{AgCl}$). All potentials are reported with respect to this reference. The approach curves were made with a platinum SECM tip (25 μm diameter). Digital simulations of the voltammograms were performed with the software package DigiSim (Bioanalytical Systems, version 2.1).

3. Results and discussion

3.1. Voltammetry at bare Au and $C_{14}SH/Au$ electrodes

The $C_{14}SH/Au$ electrode was first studied electrochemically with the hydrophilic species $\text{Fe}(\text{CN})_6^{4-}$. Indeed, this species is frequently used to probe an electrode modified by an organic thin layer and undergoes a reversible, one-electron, outer-sphere redox reaction ($E^0 = 0.153 \text{ V}$; $\alpha = 0.4$; $k^0 = 0.03 \text{ cm s}^{-1}$) [36]. Fig. 1 shows the cyclic voltammograms obtained for an aqueous solution containing $\text{Na}_4\text{Fe}(\text{CN})_6$ (1 mM) and NaCl (0.1 M) as supporting electrolyte, at bare and $C_{14}SH/Au$ electrodes. In the presence of the monolayer, the current decreased strongly and became mainly capacitive. Thioalkanes with long alkane chains are known to adsorb on gold and form a well organized, densely packed monolayer that acts as an effective electron and ion barrier [33]. Thus, in the presence of the monolayer, $\text{Fe}(\text{CN})_6^{4-}$ cannot contact the electrode surface and its apparent heterogeneous electron transfer rate, governed either by tunneling through the layer or reaction at pinholes, decreases strongly.

For quantitative analysis, we chose another compound, ferrocenemethanol with a larger standard rate constant ($E^0 = 0.154 \text{ V}$; $\alpha = 0.5$; $k^0 = 0.2 \text{ cm s}^{-1}$) [37]. Thus, even if the apparent heterogeneous electron transfer rate constants should decrease at the mono- and bilayer-modified electrode, we believed that these values should still be in a range where we could observe a significant current in the cyclic voltammogram and where these constants could be measured by SECM. The electrochemical behavior of ferrocenemethanol in aqueous solution was studied at the same electrodes (Fig. 2a and b). With a $C_{14}SH$ monolayer adsorbed on gold (Fig. 2b), the oxidation peak of ferrocenemethanol shifted from 0.18 to 0.25 V and the reduction peak from 0.12 to 0.05 V. We also observed a small decrease in the anodic

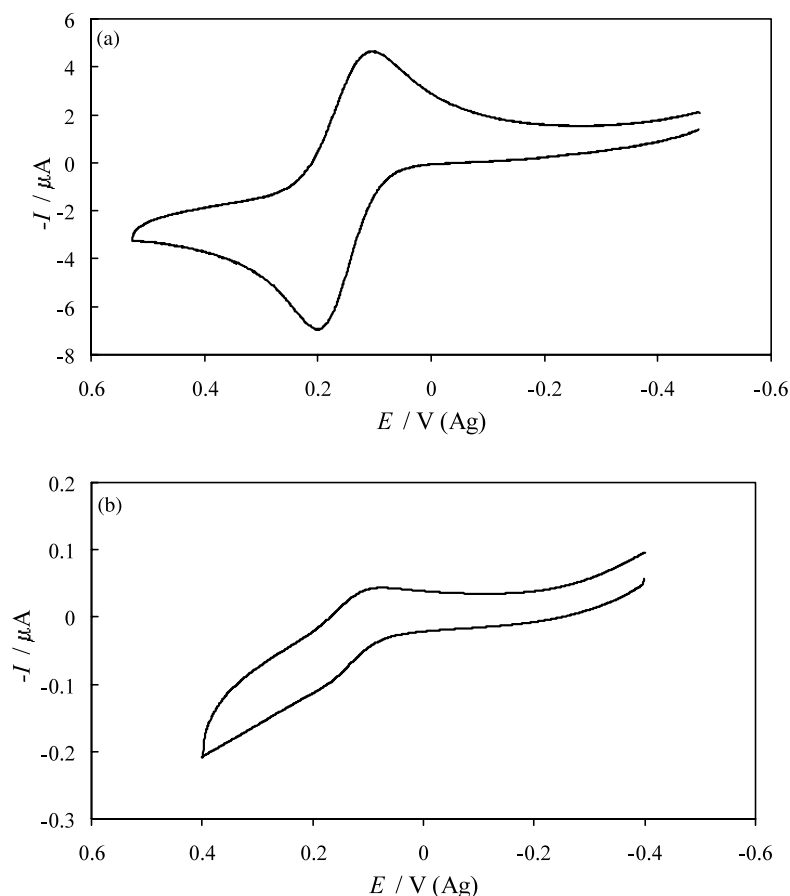


Fig. 1. Cyclic voltammograms of an aqueous solution containing $\text{Na}_4\text{Fe}(\text{CN})_6$ (1×10^{-3} M) and NaCl (0.1 M) at $v = 0.05 \text{ V s}^{-1}$ on (a) gold electrode ($S = 0.038 \text{ cm}^2$) and (b) a tetradecanethiol monolayer adsorbed on gold electrode.

peak current and a large decrease in the reverse cathodic peak current.

The electron transfer at such electrodes can occur in three ways [34]: (1) by tunneling of electrons through the monolayer; (2) by permeation of the redox species into

the monolayer followed by diffusion in the layer and electron transfer at the electrode (membrane model) and (3) by diffusion of the electroactive compound to pinhole or defect sites and ET at the electrode surface (pinhole model). The mode of reaction at a filmed

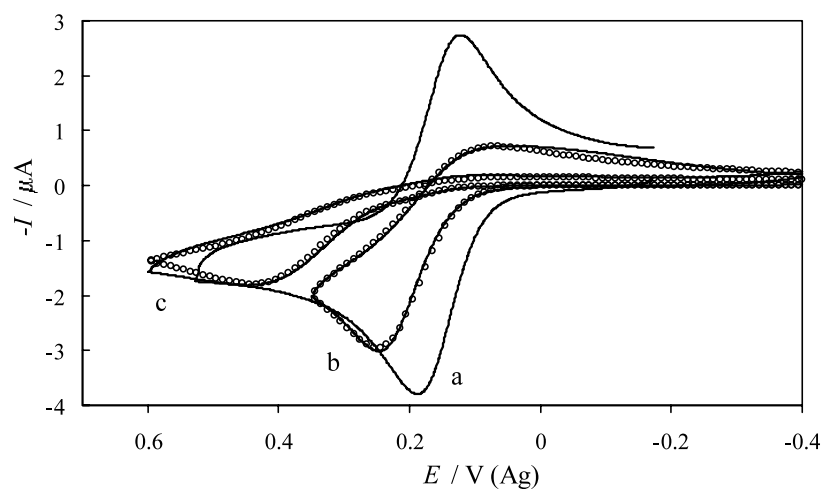


Fig. 2. Cyclic voltammograms of an aqueous solution containing ferrocenemethanol (5×10^{-4} M) and NaCl (0.1 M) at $v = 0.05 \text{ V s}^{-1}$ on (a) bare gold electrode ($S = 0.038 \text{ cm}^2$), (b) on an adsorbed tetradecanethiol monolayer and (c) on a phospholipid/tetradecanethiol bilayer adsorbed on gold electrode. The solid line corresponds to the experimental curve and the dashed line (○) to the curve obtained by simulation.

electrode can be probed by determining how the limiting current, e.g., in a voltammetric experiment, changes with time or sweep rate [38]. An alternative approach, especially useful for high coverage, is to determine how the effective heterogeneous rate constant of a reaction is affected by coverage. This is the approach taken here. For both redox couples, we estimated the apparent standard rate constant at the C₁₄SH/Au electrode by a simple Tafel plot analysis on the rising portion of the CV (Fig. 3). The apparent electron transfer rate constant was obtained from the values of the current at each potential, $I(E)$ as:

$$k_{\text{app}}(E) = \frac{I(E)}{nFAc} \quad (1)$$

with A , the electrode area and c , the substrate concentration. From extrapolation of the Tafel linear variation of $\log k_{\text{app}}(E)$ with the electrode potential, E , to the standard oxidation potential ($E = E^0$), one obtains an apparent standard electron transfer rate constant, $k_{\text{CV}}^{0,\text{mono}} = 2 \times 10^{-5} \text{ cm s}^{-1}$ for $\text{Fe}(\text{CN})_6^{4-}$. This value is about 1500 times smaller than the standard rate constant at a bare Au electrode, $k^0 = 0.03 \text{ cm s}^{-1}$.

We can estimate the apparent standard rate constant for electron transfer that occurs only by tunneling by comparing these results to those of Miller and co-workers [39–43], who investigated tunneling electron transfer at ω -hydroxythiol coated Au electrodes. This work predicts that the electron transfer rate constant would decrease exponentially with chain length of the alkyl thiol with a tunneling factor β of 0.9 per methylene unit, so that with C₁₄SH, one would predict that the apparent electron transfer rate constant is $k_{\text{tunnel}}^0 = k^0 \exp(-0.9n_{\text{Me}}) = 10^{-7} \text{ cm s}^{-1}$. Since the standard rate constant we find at the C₁₄SH/Au electrode, $k_{\text{CV}}^{0,\text{mono}}$, is much larger than the standard rate constant estimated by considering only tunneling, k_{tunnel}^0 , we

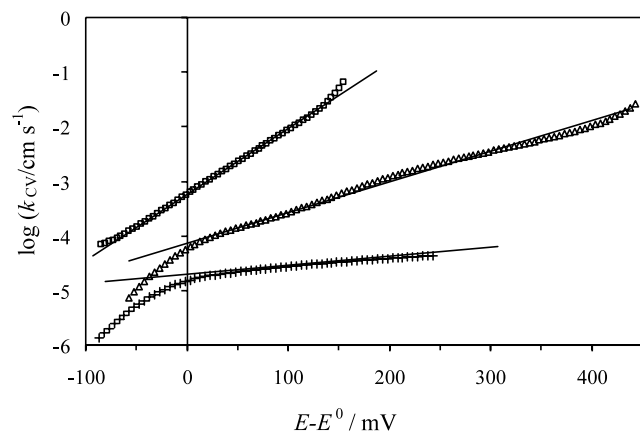


Fig. 3. Tafel plots for (◆) ferrocenemethanol at the C₁₄SH/Au electrode, (△) ferrocenemethanol at the POPC/C₁₄SH/Au electrode and (+) $\text{Fe}(\text{CN})_6^{4-}$ at C₁₄SH/Au. Solid lines according to (2) for ferrocenemethanol and (1) for $\text{Fe}(\text{CN})_6^{4-}$.

conclude that the monolayer had pinholes and that the electron transfer for ferrocyanide corresponds to oxidation at the pinholes or defect sites. Thus, the presence of these pinholes considerably enhances the current seen at the C₁₄SH/Au electrode compared to the current due only to tunneling.

A Tafel analysis was also done with ferrocenemethanol to estimate the apparent standard rate constant. For this species, since a diffusive peak is observed, the $I-E$ curve was convoluted before analysis. We assumed that the process was a quasireversible electron transfer. In this case, the variation of the apparent electron transfer rate constant with $I(E)$, the current and $\tilde{I}(E)$, the convoluted current, is given by [44–46]:

$$k(E) = \frac{I(E)}{I_{\text{lim}} - \tilde{I}(E)(1 + \exp(-nF/RT(E - E^0)))} \quad (2)$$

where I_{lim} is the diffusion limiting current of the sigmoidal convoluted current.

The variation of $\log k(E)$ with $E - E^0$ is shown in Fig. 3. The extrapolation of this Tafel plot to $E = E^0$ leads to a value of the apparent standard electron transfer rate constant, $k_{\text{CV}}^{0,\text{mono}}$ of $6 \times 10^{-4} \text{ cm s}^{-1}$. The value of the standard electron transfer rate constant at the bare gold electrode could be estimated by CV. The method consists of comparing the variation of the anodic peak half-width with the scan rate (ranging from 0.05 to 0.5 V s⁻¹) to the theoretical one for a quasi-reversible electron transfer [47]. For the scan rates investigated, the peak half-widths are on the borderline between Nernstian and quasi-reversible behavior. An approximate value of $k^0 = 0.14 \text{ cm s}^{-1}$ was estimated, of the same order of magnitude as that obtained on a glassy carbon electrode ($k^0 = 0.2 \text{ cm s}^{-1}$) [37] and its comparison with the k^0 value for the ferrocyanide oxidation is similar to that observed for these couples at a platinum electrode [48].

The rate constant measured for the ferrocenemethanol oxidation at the monolayer is then approximately 4×10^{-3} times the value of the standard electron transfer rate constant estimated at our bare Au electrode. The ratio $k_{\text{CV}}^{0,\text{mono}}/k^0$ obtained for ferrocenemethanol is 6 times higher than the ratio for ferrocyanide. However, as the k^0 value for the ferrocenemethanol oxidation is on the borderline of accessible rate constants by the CV technique, within the usual variation in measured k^0 values, the ratios of the two species are not significantly different and, could suggest, in first approximation, that the electron transfer for both redox couples at the C₁₄SH/Au electrode is governed kinetically by diffusion to defect sites [49]. Nevertheless, ferrocenemethanol is more hydrophobic than ferrocyanide and it is an uncharged compound. It is then more prone to permeate [50] into the layer than ferrocyanide.

However, at a longer adsorbed monolayer (C₁₈SH monolayer instead of C₁₄SH), no permeation of the

ferrocenemethanol has been observed [16], so we believe that, if possible at the $C_{14}SH$ adsorbed monolayer, the permeation is not the only contribution to the oxidation kinetics.

3.2. Voltammetry at POPC/ $C_{14}SH$ /Au electrode

The ferrocenemethanol cyclic voltammogram obtained at POPC/ $C_{14}SH$ /Au electrode is presented in Fig. 2c. The oxidation peak shifts from 0.18 to 0.44 V, the anodic peak current is even smaller than with the monolayer and the reduction peak disappears almost totally on the reverse scan. This can be explained by a further decrease of the apparent standard rate constant. Indeed, it is well known that, as the thickness of the layer after lipid adsorption increases, the electron transfer at a bilayer-modified electrode is blocked to an even greater extent compared to that at a monolayer-modified electrode [8–10]. To confirm these observations, we calculated the apparent standard rate constant of ferrocenemethanol at the POPC/ $C_{14}SH$ /Au electrode with the same treatment as used for the $C_{14}SH$ /Au electrode. The apparent standard rate constant at the bilayer-modified electrode obtained from the Tafel plot analysis (Fig. 3), $k_{CV}^{0,bi} = 7 \times 10^{-5} \text{ cm s}^{-1}$, is ten times smaller than the value obtained for the monolayer-modified electrode. According to these results, the ferrocenemethanol electron transfer is blocked more by the bilayer than by the monolayer and this compound should not penetrate through the bilayer.

3.3. SECM approach curves to $C_{14}SH$ /Au and POPC/ $C_{14}SH$ /Au substrates

We have also used SECM to characterize the charge transfer processes occurring at the mono- and bilayer-modified gold electrode during the reduction of ferriceniummethanol. A platinum ultra-microelectrode (UME) tip (radius, $a = 12.5 \mu\text{m}$) was used to approach the substrate. The tip potential was 0.35 V to generate the ferriceniummethanol and the substrate potential was held at -0.4 V to reduce it back to ferrocenemethanol (Fig. 4). The analytical treatment obtained to describe finite heterogeneous kinetics at the substrate could be used to describe the electrochemical process whenever it is limited by slow substrate electron transfer or by mass transport through the pinholes [26]. The expression of the tip current is then given as a function of the normalized tip-substrate separation ($L = d/a$) as:

$$I_T^k = \left[\frac{0.78377}{L(1 + 1/A)} + \frac{0.68 + 0.3315 \exp(-1.0672/L)}{1 + F(L, A)} \right] \times (1 - I_T^{\text{ins}}/I_T^c) + I_T^{\text{ins}} \quad (3)$$

where I_T^c and I_T^{ins} represent the tip currents for conductive and insulating substrates, respectively. Their

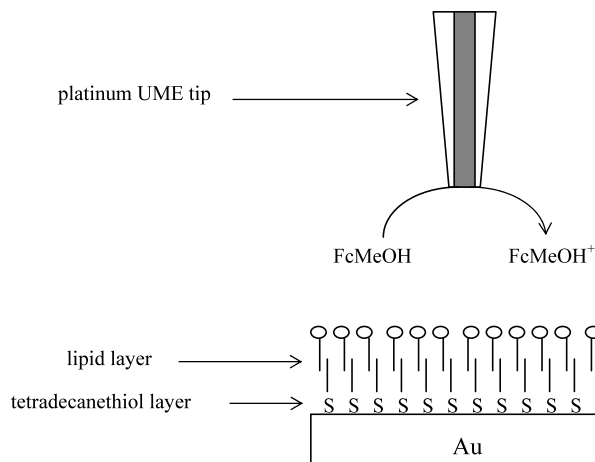


Fig. 4. Schematic representation of the SECM experiment at the filmed electrode.

expressions as functions of the normalized distance $L = d/a$ are:

$$I_T^c = 0.78377/L + 0.3315 \exp(-1.0672/L) + 0.68 \quad (4)$$

$$I_T^{\text{ins}} = 1/(0.15 + 1.5358/L + 0.58 \exp(-1.14/L) + 0.0908 \exp[(L - 6.3)/(1.017L)]) \quad (5)$$

$A = kd/D$ with k the apparent limiting heterogeneous rate constant and D the diffusion coefficient ($D = 7 \times 10^{-6} \text{ cm}^2 \text{ s}^{-1}$); and $F(L, A) = (11 + 7.3A)/A/(110 - 40L)$.

Fig. 5 shows the curves obtained with conductive (a) (Au); (b) $C_{14}SH$ /Au; (c) POPC/ $C_{14}SH$ /Au and (d) insulating substrates. Curves b and c fit the theoretical expression Eq. (3) well, when the apparent heterogeneous rate constants have the following values: for the monolayer $k_{SECM}^{0,mono} = 0.02 \text{ cm s}^{-1}$ and for the bilayer $k_{SECM}^{0,bi} = 0.0007 \text{ cm s}^{-1}$. In both cases, the values obtained by SECM are greater than the values obtained by CV. At such a high reductive substrate overpotential, the electron transfer rate constant at the bare Au electrode should be potential independent and about 10^3 times higher than the standard rate constant, k^0 [51]. Therefore, the apparent rate constant at the covered Au electrodes would be expected to be much higher than the values obtained with the SECM. Thus, under these SECM conditions, the redox process at the modified electrodes is limited by mass transport through pinholes rather than by the electron transfer rate at the substrate and the rate constant extracted from the SECM study is given by [26]:

$$k_{SECM} = \frac{4(1 - \theta)D}{\pi R_d} \quad (6)$$

where θ is the Au electrode fractional surface coverage and R_d , the equivalent radius of the pinholes (considered cylindrical).

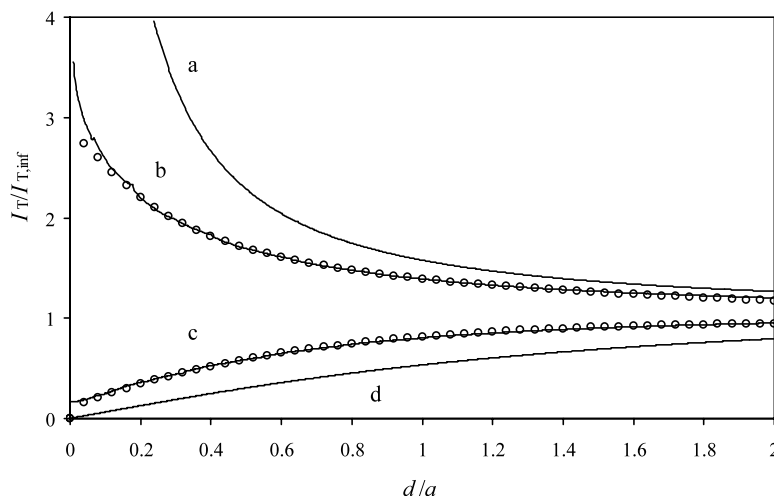


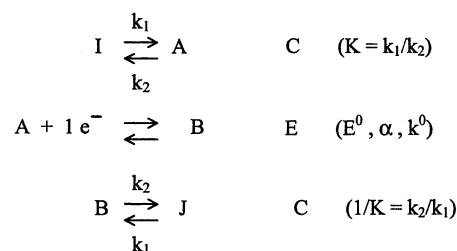
Fig. 5. Current-distance curves for a 12.5- μm -radius Pt tip UME approaching; (a) a conductive substrate; (b) a gold substrate covered by a tetradecanethiol monolayer; (c) a gold substrate covered by a phospholipid/tetradecanethiol bilayer and (d) an insulating substrate. The tip was biased at 0.35 V vs. Ag and the substrate at -0.4 V vs. Ag in an aqueous solution containing 5×10^{-4} M ferrocenemethanol and 0.1 M NaCl. The tip scan rate was $1 \mu\text{m s}^{-1}$. The solid lines correspond to the experimental curves and the dashed lines (○) to the SECM theory (Eq. (3)).

As the apparent heterogeneous rate constant obtained at the $\text{C}_{14}\text{SH}/\text{Au}$ electrode, $k_{\text{SECM}}^{0,\text{mono}}$, is larger than the value obtained at the $\text{POPC}/\text{C}_{14}\text{SH}/\text{Au}$ electrode, $k_{\text{SECM}}^{0,\text{bi}}$, the redox process is easier at the $\text{C}_{14}\text{SH}/\text{Au}$ electrode than at the $\text{POPC}/\text{C}_{14}\text{SH}/\text{Au}$ electrode. This confirms the results obtained by CV.

3.4. Cyclic voltammogram simulation

As an oxidation peak can still be observed for the ferrocenemethanol at a gold electrode modified by the mono- or bilayer, this species is a good candidate to simulate the cyclic voltammogram and give access to a quantitative analysis. The electron transfer kinetics for ferrocenemethanol at the mono- and bilayer-modified gold electrode were measured by two techniques, CV Tafel analysis and SECM approach curves, but not under exactly the same electrochemical conditions, and thus do not characterize the same electron transfer or mass transport rates. Thus, it was interesting to see to what extent these different characterizations could reproduce theoretically the CV obtained at the different electrodes. We then simulated the cyclic voltammograms using the data from both methods. Amatore et al. [49] proposed a theoretical analysis to treat cyclic voltammograms at a partially covered electrode with microscopic defects. Even if this analysis fits the experimental curves only semi-quantitatively [26], we have used it as the only one available to our knowledge, to simulate our experiments. According to the authors, the electron transfer process at such an electrode can be simulated by a CEC mechanism (Scheme 1).

In this scheme the electron transfer corresponds to the ET at the metallic surface of the uncovered electrode sites (defects) and the preceding and succeeding reaction



Scheme 1.

corresponds physically to diffusion of the reactants into the pinholes defined as the defects. The preceding and the following chemical reactions have the same thermodynamic and kinetic parameters, and the electron transfer rate is the same as that at the bare electrode. This mechanism is governed by two dimensionless parameters:

$$K\sqrt{\lambda} = 1.67 \sqrt{\frac{DRT}{Fv} \frac{(1-\theta)}{R_d}} \quad (7)$$

and

$$\Lambda(1-\theta) = \sqrt{\frac{RT}{FvD}} k^0 (1-\theta) \quad (8)$$

with $\lambda = (k_1 + k_2)RT/Fv$; $K = (1-\theta)/\theta$.

A zone diagram was established as a function of these two parameters. According to this diagram, because the ferrocenemethanol cyclic voltammograms at $\text{C}_{14}\text{SH}/\text{Au}$ electrode and $\text{POPC}/\text{C}_{14}\text{SH}/\text{Au}$ electrodes present a diffusive peak, the parameter $K\sqrt{\lambda}$ is greater than 1. Thus, the electrode coverage results in an apparent decrease of the electron transfer kinetic and the apparent standard rate constant (measured by CV at $E = E^0$)

can be expressed as:

$$k_{CV}^0 = k^0(1 - \theta) = k^0 K = k^0 k_1 / k_2 \quad (\text{when } \theta \rightarrow 1) \quad (9)$$

As we have measured the apparent standard rate constants ($k_{CV}^{0, \text{mono}}$ and $k_{CV}^{0, \text{bi}}$) from the Tafel analysis, we have extracted the effective chemical equilibrium constant, K (see Table 1).

Under the SECM experimental conditions, the overpotential is high enough to be limited by mass transfer inside the pinholes and not by electron transfer. Thus Eq. (7) can be rewritten as a function of the apparent rate constant (k_{SECM}^0) obtained in this case:

$$K\sqrt{\lambda} = 1.67\sqrt{\frac{DRT}{Fv}} \frac{\pi k_{SECM}^0}{4D} \quad (10)$$

$$K\sqrt{k_1 + k_2} = 1.67 \frac{\pi k_{SECM}^0}{4\sqrt{D}} \quad (11)$$

Therefore, the kinetic constants k_1 and k_2 were calculated from Eq. (9) and Eq. (11) and the values obtained were used to start the cyclic voltammogram simulation (see Table 1).

Taking into account the approximations made in the treatment (i.e. the simple description of the geometry of the pinholes), we can conclude that for the monolayer-modified electrode, the values obtained by simulation were in good agreement with those calculated, except for the kinetic rate constants of the following reaction. These constants had to be decreased in order to fit well the loss of reversibility at the reverse scan (Fig. 2b). This could reflect possible permeation of the ferrocenemethanol and a lesser permeation and then stability, because of its ionic character, in the monolayer of the ferriceniummethanol formed at the electrode. Cleaner evidence of such a phenomenon has been discussed in the case of menadione permeation at a monolayer covered electrode [50]. In this work, a mathematical model was proposed to estimate the permeability by cyclic voltammetric simulation. The ferrocenemethanol permeability in the C₁₄SH monolayer obtained by this previous model was $1.3 \times 10^{-3} \text{ cm s}^{-1}$. This value is smaller than the menadione permeability in a C₁₈SH monolayer at pH < 7 but higher than the value obtained at pH > 7

which rather characterizes transport through pinholes. We have concluded that the menadione permeability is low at basic pH. By analogy, we could assume that the ferrocenemethanol could permeate the monolayer to a small extent.

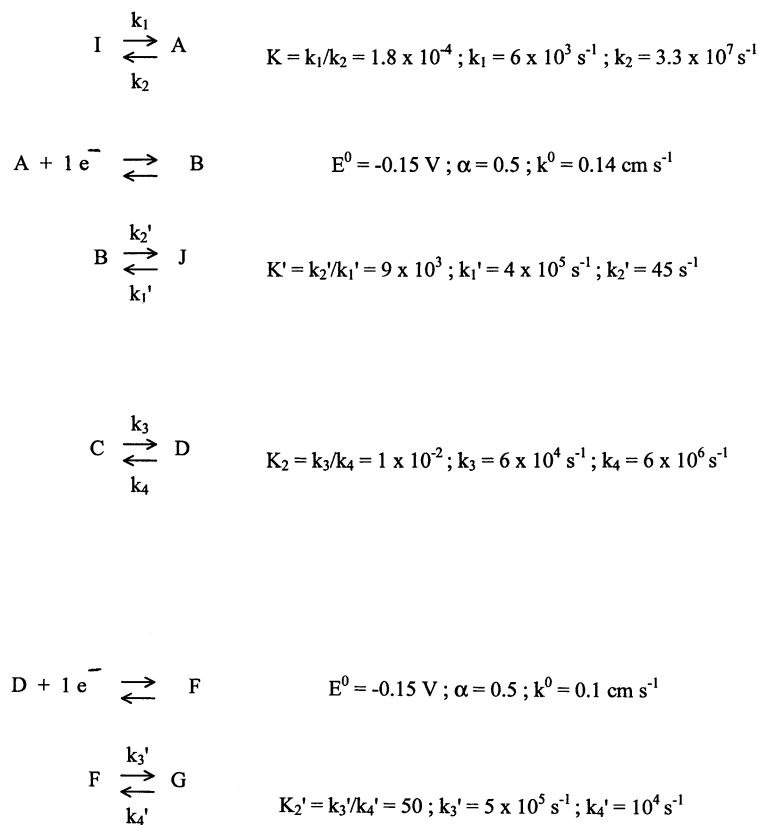
For the bilayer-modified electrode, we could fit the curve with values close to those calculated with respect to the chemical equilibrium constant, K . For the kinetic constants, k_1 and k_2 , we had to change the calculated values to fit the curve well (Fig. 2c). The same argument concerning the approximations made in the theoretical treatment could be invoked, but we could also assume that the difference in these kinetic constants could reflect specific interactions between the second layer and the electroactive species, since the phospholipid contains functional groups. Nevertheless, in this case the differences between the values obtained by simulation and calculation are smaller in the case of the bilayer than in the case of the monolayer for the following reaction. Then, we could assume that ferrocenemethanol permeated the bilayer to a much lesser extent because of interactions with the functional groups contained into the phospholipids. This can be proved by the smaller value of $k_{CV, \text{perm}} = 1.9 \times 10^{-4} \text{ cm s}^{-1}$ obtained from the CV if the permeation model is assumed.

Furthermore, the cyclic voltammogram shows a shoulder that could not be fit with the simple CEC mechanism. We attribute this shoulder to the oxidation of ferrocenemethanol at sites where the phospholipids are not adsorbed on the tetradecanethiol layer. As the current corresponding to this contribution is small (< 10% of the total current), we have assumed that the surface area of these sites, not covered by lipid, is small compared to the total covered area. To account for this effect, we have added a second CEC mechanism involving a species with the same electron transfer parameters (E^0 , α , k^0) but with a smaller concentration (see Scheme 2). The first three reactions (artificial species I, A, B and J) correspond to the ET through an ideal bilayer possessing pinholes, as discussed for Scheme 1. The three others (artificial species C, D, F and G) account for the portion of ferrocenemethanol that does not sense the bilayer, and it will characterize the ET

Table 1

Values of equilibrium and kinetic constants calculated from Eq. (9) and Eq. (11) and obtained by simulation using a CEC mechanism, for the Au electrode modified by a mono- or bilayer

	For the monolayer		For the bilayer	
	Calculated values	Values obtained by simulation	Calculated values	Values obtained by simulation
$10^3 K$	3	7	0.35	0.18
$10^{-5} k_1/s^{-1}$	0.3	3	0.0035	0.06
$10^{-7} k_2/s^{-1}$	1	4.3	0.1	3.3
K'	333	160	2860	9000
$10^{-6} k_1'/s^{-1}$	10	0.006	1	0.4
$10^{-2} k_2'/s^{-1}$	300	0.38	3.5	0.45



and $[I] = 5.7 \times 10^{-4} \text{ M}$ and $[C] = 3 \times 10^{-5} \text{ M}$

Scheme 2.

at sites covered by the monolayer but not by the phospholipids.

To fit the curve well, we had to consider both preceding and following chemical reactions. Therefore, this oxidation occurs at a monolayer-modified surface and not at a bare electrode. The ratio of the concentrations of the two species corresponds, in fact, to the ratio of the surface covered by the bilayer and the surface covered by a monolayer only. So we have estimated that 5% of the overall surface of the monolayer-modified electrode has not been covered by phospholipids. This surface area would correspond roughly to the total area damaged by the three approach curves we performed to characterize the monolayer. Actually, the establishment of the approach curves implies, in the end, a physical contact between the tip and the substrate.

Finally, from the values obtained by simulation and by using Eq. (12), the surface coverage has been measured: θ is equal to 0.9998 for the bilayer, close to the approximate value we estimate from the ferrocyanide oxidation at the monolayer (0.9993) or from that found for C_{18}SH monolayer (0.99995) [50]

$$K = (1 - \theta)/\theta \quad (12)$$

In the case of the monolayer, assuming that there is

no permeation, the value of 0.993 obtained from Eq. (12) represents the minimal surface coverage of the electrode.

Therefore, even if 5% of the total surface of the monolayer covered electrode is damaged by the approach curves, the surface coverage increases well after the adsorption of the phospholipids on the monolayer. Despite the roughness of the gold surface electrode (gold wire inserted in Teflon is easier to characterize by SECM), we find that the surface coverage is still high for the monolayer and the bilayer.

4. Conclusion

The results confirm that the self-assembly method allows the easy preparation of stable mono- and bilayers supported on gold. The surface coverages, calculated from the values obtained by simulation, are higher than 0.993 for the monolayer and 0.9998 for the bilayer. This coverage is high enough to induce a large decrease of the apparent standard rate constant and this decrease is even larger in the case of the bilayer. The estimated apparent standard rate constants indicate that ferrocenemethanol electron transfer at the mono- and bilayer-

modified electrodes does not occur by tunneling, but rather by diffusion through the pinholes with electron transfer at the free sites of the electrode. We have also concluded that the ferrocenemethanol, a hydrophobic species, could permeate the monolayer to a small extent but the bilayer to a much lesser extent. The kinetics of ferrocenemethanol electron transfer at a mono- and a bilayer-modified gold electrode could be measured by CV or SECM. Indeed, the values obtained by these two techniques were close to the values obtained by simulation. The differences observed could be due to the approximations made in the treatment (i.e. the simple description of the geometry of the pinholes). The differences could be due also to partial permeation of the ferrocenemethanol and instability of the ionic ferriceniummethanol in the monolayer. The permeation into the bilayer seems less efficient where the electron transfer is governed more by the pinhole contribution. Future work will focus on the extension of this kinetic treatment to species that can permeate the mono- and the bilayers, our final goal being to analyze real biological membranes and systems such as yeast cells.

Acknowledgements

The support of this work by grants from IGEN, the National Science Foundation (CHE-9870762), and the Robert A. Welch Foundation is gratefully acknowledged.

References

- [1] J.N. Robinson, D.J. Cole-Hamilton, *Chem. Soc. Rev.* 20 (1991) 49.
- [2] V.F. Antonov, Y.G. Rovin, L.T. Trofimov, in: *A Bibliography of Bilayer Lipid Membranes*, All Union Institute for Scientific and Technical Information, Moscow, 1979.
- [3] A. Ulman, *An Introduction to Ultrathin Organic Films: From Langmuir Blodgett to Self-Assembly*, Academic Press, Boston, 1991.
- [4] G. Puu, I. Gustafson, P.-A. Ohlsson, G. Olofsson, A. Sellström, in: J.C. Gomez-Fernandez, D. Chapman, L. Racker (Eds.), *Progress in Membrane Technology*, Birkhäuser, Basel, 1991, p. 279.
- [5] M. Kühner, R. Tampe, E. Sackmann, *Biophys. J.* 67 (1994) 217.
- [6] H.Ti. Tien, Z. Salamon, *Bioelectrochem. Bioenerg.* 22 (1989) 211.
- [7] Z. Salamon, F.K. Gleason, G. Tollin, *Arch. Biochem. Biophys.* 299 (1992) 193.
- [8] A.L. Plant, *Langmuir* 9 (1993) 2764.
- [9] A.L. Plant, M. Gueguetchkeri, W. Yap, *Biophys. J.* 67 (1994) 1126.
- [10] J.-M. Laval, M. Majda, *Thin Solid Films* 244 (1994) 836.
- [11] R. Naumann, A. Jonczyk, R. Kopp, J. van Esch, H. Ringsdorf, W. Knoll, P. Gräber, *Angew. Chem. Int. Ed. Engl.* 34 (1995) 2056.
- [12] A.L. Plant, M. Brigham-Burke, E.C. Petrella, D.J. O'Shannessy, *Anal. Biochem.* 226 (1995) 342.
- [13] J. Li, L. Ding, E. Wang, S. Dong, *J. Electroanal. Chem.* 414 (1996) 17.
- [14] R. Naumann, A. Jonczyk, C. Hampel, H. Ringsdorf, W. Knoll, N. Bunjes, P. Gräber, *Bioelectrochem. Bioenerg.* 42 (1997) 241.
- [15] S. Lingler, I. Rubinstein, W. Knoll, A. Offenhäuser, *Langmuir* 13 (1997) 7085.
- [16] O. Pierrat, N. Lechat, C. Bourdillon, J.-M. Laval, *Langmuir* 13 (1997) 4112.
- [17] J.D. Burgess, M.C. Rhoten, F.M. Hawkrigde, *Langmuir* 14 (1998) 2467.
- [18] J. Ha, C.S. Henry, I. Fritsch, *Langmuir* 14 (1998) 5850.
- [19] A.L. Plant, *Langmuir* 15 (1999) 5128.
- [20] M.A. Tarek, K. Tu, M.L. Klein, D.J. Tobias, *Biophys. J.* 77 (1999) 964.
- [21] P. Kryszynski, M.R. Moncelli, F. Tadini-Buoninsegni, *Electrochim. Acta* 45 (2000) 1885.
- [22] J. Kwak, F.C. Anson, *Anal. Chem.* 64 (1992) 250.
- [23] C. Lee, F.C. Anson, *Anal. Chem.* 64 (1992) 528.
- [24] M. Arca, M.V. Mirkin, A.J. Bard, *J. Phys. Chem.* 99 (1995) 5040.
- [25] M.E. Williams, K.J. Stevenson, A.M. Massari, J.T. Hupp, *Anal. Chem.* 72 (2000) 3122.
- [26] F. Forouzan, A.J. Bard, M.V. Mirkin, *Isr. J. Chem.* 37 (1997) 155.
- [27] G. Wittstock, R. Hesse, W. Schuhmann, *Electroanalysis* 9 (1997) 746.
- [28] G. Wittstock, W. Schuhmann, *Anal. Chem.* 69 (1997) 5059.
- [29] M. Tsionsky, A.J. Bard, M.V. Mirkin, *J. Am. Chem. Soc.* 119 (1997) 10785.
- [30] M. Tsionsky, J. Zhou, S. Amemiya, F.-R.F. Fan, A.J. Bard, R.A.W. Dryfe, *Anal. Chem.* 71 (1999) 4300.
- [31] S. Amemiya, Z. Ding, J. Zhou, A.J. Bard, *J. Electroanal. Chem.* 483 (2000) 7.
- [32] S. Amemiya, A.J. Bard, *Anal. Chem.* 72 (2000) 4940.
- [33] C.J. Slevin, S. Ryley, D.J. Walton, P.R. Unwin, *Langmuir* 14 (1998) 5331.
- [34] M.D. Porter, T.B. Bright, D.L. Allara, C.E.D. Chidsey, *J. Am. Chem. Soc.* 109 (1987) 3559.
- [35] C.D. Bain, E.B. Troughton, Y.-T. Tao, J. Evall, G.M. Whitesides, R.G. Nuzzo, *J. Am. Chem. Soc.* 111 (1989) 321.
- [36] V. Marecek, Z. Samec, J. Weber, *J. Electroanal. Chem.* 94 (1978) 169.
- [37] C. Bourdillon, C. Demaille, J. Moiroux, J.-M. Savéant, *J. Am. Chem. Soc.* 117 (1995) 11499.
- [38] A.J. Bard, L.R. Faulkner, *Electrochemical Methods, Fundamentals and Application*, second ed., Wiley, New York, 2001, pp. 619–623.
- [39] C. Miller, P. Cuendet, M. Grätzel, *J. Phys. Chem.* 95 (1991) 877.
- [40] C. Miller, M. Grätzel, *J. Phys. Chem.* 95 (1991) 5225.
- [41] A.M. Becka, C. Miller, *J. Phys. Chem.* 96 (1992) 2657.
- [42] A.M. Becka, C. Miller, *J. Phys. Chem.* 97 (1993) 6233.
- [43] S. Terrettaz, A.M. Becka, M.J. Traub, J.C. Fettingier, C. Miller, *J. Phys. Chem.* 99 (1995) 11216.
- [44] J.C. Imbeaux, J.-M. Savéant, *J. Electroanal. Chem.* 44 (1973) 169.
- [45] J.-M. Savéant, D. Tessier, *J. Electroanal. Chem.* 65 (1975) 57.
- [46] A.J. Bard, L.R. Faulkner, *Electrochemical Methods, Fundamentals and Application*, second ed., Wiley, New York, 2001, p. 250.
- [47] L. Nadjo, J.-M. Savéant, *J. Electroanal. Chem.* 48 (1973) 113.
- [48] T. Saji, Y. Maruyama, S. Aoyagui, *J. Electroanal. Chem.* 86 (1978) 219.
- [49] C. Amatore, J.-M. Savéant, D. Tessier, *J. Electroanal. Chem.* 147 (1983) 39.
- [50] C. Cannes, F. Kanoufi, A.J. Bard, *Langmuir* 18 (2002) 8134.
- [51] R.A. Marcus, *J. Chem. Phys.* 24 (1956) 4966.